Environmental Science
Water Research & Technology

ROYAL SOCIETY OF CHEMISTRY

PAPER

View Article Online
View Journal

Cite this: DOI: 10.1039/d6ew00221h

Characterizing the impact of geometry on the performance of inline-coagulation pretreatment systems with helical flocculators

Joseph D. Ladouceur, *[a] Roberto M. Narbaitz [a] and Christopher Q. Lan[b]

Inline-coagulation (C-IN), where coagulant is added to the feed without solids separation prior to filtration, is a widely applied pretreatment strategy for low-pressure membrane fouling mitigation. At bench-scale, simulating C-IN has proven difficult due to the low flowrates involved. One promising approach to achieve continuous-flow operation in these small-scale systems is the helically coiled tube flocculator (HCTF), a coiled section of pipe. However, the impact of changing helical geometry on the properties of flocs formed by HCTFs, which can significantly affect membrane performance, has yet to be quantitatively characterized. Moreover, there are currently no widely accepted design guidelines for HCTFs. Accordingly, the current study uses a continuous-flow bench-scale system and a 2^3 full-factorial experimental design approach to investigate the impact of HCTF geometry on the properties of flocs produced. The results showed that the floc size and concentration were most significantly impacted by the pipe length (*i.e.*, retention time), while the floc fractal dimension demonstrated a relative insensitivity to helical geometry for all tested configurations. The Reynolds number was also shown to exert a critical impact on the properties of flocs, likely the result of a trade-off between mixing strength and retention time. When compared to a batch-reactor, the tested HCTF configurations produced smaller sized flocs in greater concentrations, while relative to a commercial inline static mixer, HCTFs yielded larger sized flocs in lower concentrations. The size of the flocs formed indicate that HCTFs are suitable for continuous-flow C-IN, with pipe length and system hydrodynamics being the most important parameters in their design. Additionally, the choice of mixer type significantly impacts floc properties, which are expected to alter the performance of downstream unit operations.

Received 27th February 2026,
Accepted 26th May 2026

DOI: 10.1039/d6ew00221h

rsc.li/es-water

Water impact

This work demonstrated the effectiveness of helical flocculators for low-flowrate, continuous-flow coagulation/flocculation, which presents significant challenges. Practical design guidance was provided in terms of generalizable hydrodynamic parameters and helical geometry, whose impact on floc properties was characterized for the first time. These guidelines should be tested at larger scale. Comparison with alternative mixer types provided insight supporting informed flocculator selection.

1. Introduction

Low-pressure membrane (LPM) technologies for drinking water treatment have benefitted from rapid growth over the past two decades owing to their numerous advantages.[1–3] Membrane fouling, however, which leads to a loss of productivity with time, is one of the main impediments preventing a more widespread application of LPMs in potable water treatment.[4,5] To help mitigate the fouling of LPMs, which is primarily caused by natural organic matter (NOM),[6–8] coagulation pretreatment has been established as an effective strategy capable of removing organics across a wide range of molecular weights and surface functional groups.[9] While coagulation pretreatment can be performed in a number of different configurations both with and without particle separation,[10,11] inline coagulation (C-IN), where the flocs are delivered to the membrane surface without pre-separation, has become the most popular approach owing to its reduced process complexity and smaller footprint.[12,13]

The popularity of C-IN pretreatment has garnered increased attention among academic studies and industrial

[a] Dept. Civil Eng., Univ. Ottawa, 161 Louis Paster Pvt., K1N 6N5, Ottawa, ON, Canada. E-mail: jlado088@uottawa.ca, narbaitz@uottawa.ca
[b] Dept. Chem. Biol. Eng., Univ. Ottawa, 161 Louis Paster Pvt., K1N 6N5, Ottawa, ON, Canada. E-mail: Christopher.Lan@uottawa.ca

research and design, however, simulating the continuous-flow operation of full-scale facilities at bench-scale has proven very challenging due to the low flow rates that can be managed by small-scale filtration processes.[14] As a result, a number of studies have performed coagulation using a batch-wise approach,[15–17] which is experimentally simpler to implement compared to continuous-flow systems. In such batch configurations, the feed tank/reactors had to be continuously stirred for the entire duration of the test to prevent floc settling, meaning the flocs were subjected to moderately high shear rates for considerably longer durations than typical of full-scale practice. To address this limitation, Malkoske *et al.*[14] developed a modified jar test apparatus to simulate bench-scale continuous-flow C-IN. Although effective, the flowrate required to maintain reasonable hydraulic retention times (HRT) in the coagulation and flocculation jars was much larger than that needed to operate the downstream LPMs at conventional/reasonable flux rates (owing to the small membrane surface areas used at bench-scale). Consequently, over 96% of the coagulated feed water had to be wasted. Therefore, there is a need for an effective, low-cost alternative that can simulate the continuous-flow operation of C-IN pretreatment from full-scale facilities at the low flow rates used for bench-scale LPM studies.

To this end, helically coiled tube flocculators (HCTFs), a helically wound pipe (Fig. 1), represent a promising option due to their reported ability to achieve complete and efficient mixing even when operated firmly within the laminar flow range, which is expected for small-scale studies.[18–20] This feature of HCTFs stems from the presence of strong secondary flows, that is, fluid flow towards the outer radius of curvature, normal to the direction of flow. This causes bifurcation of the flow and the formation of a pair of recirculating vortices.[21] HCTFs further offer flexibility in design for bench-scale operations as their structural simplicity allows them to be easily fabricated with any geometry based on the needs of the user. However, the helical coil geometry, including the coil pitch (p), coil diameter (d_c), and pipe diameter (d_p), has been shown to alter the hydrodynamic flow pattern within the flocculator,[19,22–27] which is expected to influence the properties of flocculated aggregates. Several studies[28–30] have reported altered floc settleability, which is known to be dependent on both the size and morphology (*i.e.*, fractal dimension) of the formed flocs,[31,32] as a result of changing helical coil geometry. To date, however, only a single study[33] has reported how changing HCTF geometry impacts floc size and none have characterized the impact on floc structure.

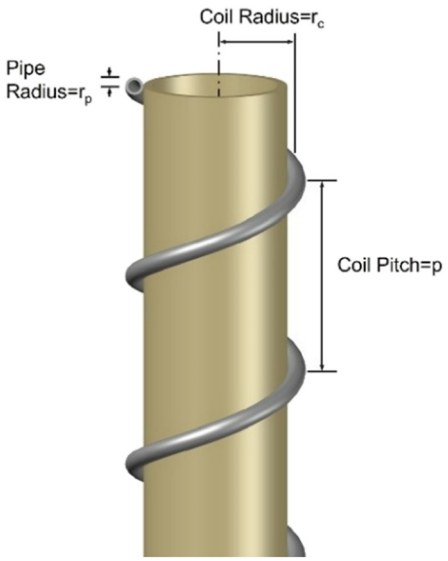

Fig. 1 Geometrical description of a helically coiled tube flocculator (HCTF).

Given the relatively large number of geometric and hydraulic parameters shown to affect the overall performance of HCTFs, a designed experiment is necessary to elucidate the relative importance of these parameters on the properties of flocs formed by the HCTF. Moreover, understanding the relationship between HCTF geometry and floc properties is critical for its application within integrated systems. For example, in the C-IN–LPM system, it is well understood that cake properties, which are significantly impacted by the size and fractal dimension of the formed floc aggregates, dictate the degree of LPM fouling.[34–38] Although HCTFs offer considerable advantages over conventional flocculators, including markedly reduced HRTs and footprints as well as the possibility for low-energy mixing at full-scale,[29,39] there remains a lack of clear design guidance for their application as part of continuous-flow coagulation-based systems.

Accordingly, the objectives of the current study were to: (a) demonstrate that continuous-flow C-IN in low flow bench-scale systems can be achieved using HCTFs; (b) employ a designed experimental approach to identify which geometric and operational properties of the HCTF exert the greatest impact on the characteristics of the formed flocs, including their size and structure, and to; (c) directly compare the properties of the flocs generated by HCTFs with those formed by alternative coagulation/flocculation strategies used in bench-scale studies, including a commercial inline static mixer (ISM) and batch reactor with vertical shaft turbine. The novelty of this study is that it is the first to comprehensively characterize the impact of helical geometry on the properties of flocs formed by HCTFs. Furthermore, a comparison between the performance of different C-IN mixing conditions is expected to provide important guidance for future researchers conducting continuous-flow lab-scale coagulation as pretreatment for different separation processes such as LPMs, sedimentation, dissolved air flotation, *etc.*

2. Materials and methods

2.1. Synthetic water

To eliminate the possibility for inter- and intra-annual variations in water quality typical of natural water sources,[40] a synthetic water was prepared by combining stock solutions of humic acid (HA) (H16752, Sigma-Aldrich, St. Louis, MO),

bovine serum albumin (BSA) (A7906, Sigma-Aldrich, St. Louis, MO), and sodium alginate (SA) (180 947, Sigma-Aldrich, St. Louis, MO), which were selected to represent humic substances, proteins, and polysaccharides, respectively. These model foulants have been previously used by a number of studies to simulate the organic matrix of natural waters.[41,42] Details regarding the preparation of the model organic stock solutions are presented in the SI (section S1).

The applied concentration of each model organic component was 5 mg L^{-1} HA, 4 mg L^{-1} BSA, and 4 mg L^{-1} SA yielding a water with a dissolved organic carbon (DOC) content of approximately 5 mg-C per L, which is within the range of typical concentrations for natural surface waters,[43] and a moderate hydrophobicity, as defined by the specific ultraviolet absorbance at 254 nm (SUVA).[44] To simulate the more complex nature of natural waters, kaolin clay (~5 mg L^{-1}, corresponding to a turbidity of 5.5 NTU, Laboratory Grade 75185, Fisher Scientific, Hampton, NH), calcium chloride (0.6 mM, 97%, Thermo Scientific, Hampton, NH), and sodium bicarbonate (0.9 mM, Certified ACS, Fisher Scientific, Hampton, NH) were added to provide low levels of turbidity, hardness, and alkalinity, respectively.[45] Prior to commencing any testing, the pH of the raw water was adjusted to 7.5 and the turbidity was verified using a turbidimeter (2100AN, Hach, Loveland, CO). A summary of the key organic and inorganic characteristics of the synthetic water is provided in Table 1.

2.2. Experimental procedure

The effects of HCTF geometry as well as coagulation chemistry, which are expected to influence the properties of the formed flocs, were initially screened using an unreplicated fractional factorial design of resolution IV (2^{6-2}_{IV}). This design was selected because the six main effects are confounded only with three-factor or higher interactions (not with two-factor interactions), which are almost always small in magnitude and can be neglected, allowing clear estimation of the main effects of each factor using only 16 tests.[46] Based on these results, the HCTF geometrical factors with the greatest significance were further studied using a two-level full-factorial design (FFD) to characterize their effects on floc size, structure (fractal dimension), and concentration. Finally, the properties of flocs formed by the various HCTF geometries in the full factorial study were compared with those formed by a commercial ISM using the same continuous-flow C-IN system, as well as flocs formed by batch coagulation using a conventional jar test apparatus. Details regarding the designed experiments, the continuous-flow bench-scale system, and the characterization of flocs are provided in the subsequent sections. Due to space limitations, details regarding the design and outcome of the preliminary screening experiments are presented in the SI (section S2).

2.2.1. Full-factorial study. The full-factorial experiments considered a replicated 2^3 design with three center points (*i.e.*, factors are set midway between their low and high levels), yielding a total of 22 runs. Based on the results of the screening study, the coil pitch (x_1), pipe length (x_2), and coil diameter (x_3) were chosen as HCTF geometrical factors of interest. The high and low factor settings for the coil pitch and coil diameter were typical of reported values from the literature[19,28,29] and selected to be within the range of Pareto-optimal values identified in the study by Mansour *et al.*[47] The pipe diameter was fixed at 3.175 mm (1/8″) as, from a practical perspective, the small cross-section helped to prevent settling of flocs within the pipe due to the higher axial flow velocity. Moreover, fixing the pipe diameter also constrained the range of theoretical HRT values between 1.6–3.2 min for the chosen pipe lengths (Table S1), thereby reducing its potential confounding effects on floc properties. While the geometric factors were selected based on the practical considerations noted above, it must be acknowledged that changes in their values did not affect the mean velocity gradient (*i.e.*, G value), which remained ~18 s^{-1} (according to the model by Tse *et al.*[48]) for all tested configurations. Although floc properties are also dependent on coagulant type,[49] alum (see Table S2, ALS, Kemira, Varennes, QC) was used throughout this study to minimize the number of tests and because it was shown to have a high efficiency for this synthetic water type, yielding equally good zeta potential and DOC reduction as specialty blend pre-polymerized types (see Fig. S1). Despite the coagulation chemistry being shown to exert an important influence on floc properties during preliminary screening experiments (see Tables S5–S7), the objectives of the current study were to characterize the impact of helical geometry on floc properties. Accordingly, for the FFD, the alum coagulant dose and pH were fixed at 3 mg-Al per L and 6, respectively, corresponding to the jar test optimal conditions for this synthetic water (Fig. S2). A summary of the factor settings for the FFD is provided in Table 2.

The response variables were selected to characterize the floc size and structure (fractal dimension), which were shown

Table 1 Synthetic water quality

		Organic measures			Inorganic measures		
Parameter	pH (unit)	DOC (mg-C per L)	UV_{254} (cm^{-1})	SUVA (L mg^{-1} m^{-1})	Turbidity (NTU)	Hardness (mg-$CaCO_3$ per L)	Alkalinity (mg-$CaCO_3$ per L^{-1})
	7.52 ± 0.05	4.98 ± 0.01	0.108 ± 0.006	2.17 ± 0.12	5.44 ± 0.08	61.83 ± 0.53	52.17 ± 2.27

Note: ± represents the 95% confidence interval calculated based on two-tailed Students *t*-test, $\mu \pm t_{0.025,n}\frac{s}{\sqrt{n}}$.

Table 2 Factor level settings for 2^3 FFD

Factors	Unit	Levels (−1)	(0)	(+1)
x_1: Coil pitch	(mm)	15	30	45
x_2: Pipe length	(mm)	1000	1500	2000
x_3: Coil diameter	(mm)	50	67.5	75

by others to be impacted by changing HCTF geometry, as well as the floc concentration, which was reported by Malkoske *et al.*[14] to impact the reversibility of the fouling layer in LPM systems. Details regarding the calculation of these floc properties are provided in section 2.4. The general form of the regression model used for the 2^k factorial design is given in eqn (1):[46]

$$y = \beta_0 + \sum_{i}^{k} \beta_i x_i + \sum \sum_{i<j=2}^{k} \beta_{ij} x_i x_j + \varepsilon \quad (1)$$

where: y is the response variable, β_0 is the intercept, β_i is the regression coefficient for the ith predictor variable (factor), β_{ij} is the regression coefficient for the interaction of factors i and j ($i \neq j$), x_i is the predictor variable (factor), and ε is the random error component. In this study, the response variables include the floc size (measured as the equivalent circular diameter (ECD)), floc concentration, and fractal dimension, the calculation of which is described in section 2.4.2.

2.2.2. Bench-scale coagulation systems. Continuous-flow C-IN by the HCTFs, as well as a commercial ISM, was evaluated using the bench-scale system shown in Fig. 2. The synthetic water was stored in a glass reservoir positioned on a magnetic stirrer in order to prevent settling of the suspended clay particles. A precision metering pump (Optos 3HM, Eldex, Napa, CA) was used to withdraw the feedwater from the reservoir through 3.175 mm (1/8″) stainless steel piping (SS-T2-S-028-20, Swagelok, Solon, OH) at a flowrate of 5 mL min^{-1} (Re = 33.3), which is low but representative of flowrates encountered in bench-scale LPM studies.[15,16] After passing through a pulse dampener (MFLX0759620, Avantor Inc., Radnor, PA), coagulant was added inline at a junction just upstream of the mixer using a syringe pump (Pump 22, Harvard Apparatus, Cambridge, MA), which was required for accurate delivery of low volumes of coagulant. The ISM was purchased from Koflo Corporation and had a 316 L stainless steel housing with an inside diameter of 8.1 mm (~5/16″) and 21 helical elements (3/8–21, Koflo, Cary, IL). The mean G-value for the ISM was estimated to be 25.8 s^{-1} based on differential pressure measurements (see section S3). HCTFs were manufactured in-house with varying geometries defined by the fractional- and full-factorial designs. The polyethylene tubing was wound around a central acrylonitrile butadiene styrene pipe, which ensured a constant coil diameter, and was affixed at pre-measured locations according to the HCTF pitch. Prior to the sampling of flocs for a given test condition, the system was allowed to run for a period of 1 h to achieve steady-state floc properties, which is in excess of the 5 HRTs required to achieve steady state operation in continuous-flow reactors noted by Malkoske *et al.*[14] and Crittenden *et al.*[43] for constant rate kinetics.

For batch coagulation tests, a conventional jar test apparatus was used (Model 7790-400, Phipps and Bird, Richmond, VA). Coagulant was added to the gator jar and rapid mixed for 2 min at 164 rpm ($G \sim 296$ s^{-1}) prior to the mixer speed being reduced to 127 rpm to provide a constant mean velocity gradient of 200 s^{-1} (to prevent floc settling) for the duration of the test. Mixer speeds were calculated according to the model presented by Bratby[50] to match the G values used in our previous batch coagulation study[16] and are representative of the conditions used by previous bench-scale LPM studies with coagulation performed by batch reactors.[17,51,52] As LPM tests with pretreatment by C-IN using batch coagulation involve significantly longer HRTs than for continuous-flow systems, floc samples were collected and analysed every 60 min over a period of 3 h to evaluate whether the constant mixing led to kinetic changes in floc properties.

2.3. HCTF geometrical characterization

While the factorial analysis in this study considered the coil pitch, coil diameter, and pipe length as factors describing HCTF geometry, many previous studies have related the flow hydrodynamics in coiled pipes to the degree of curvature, which measures the within-plane deviation from a straight

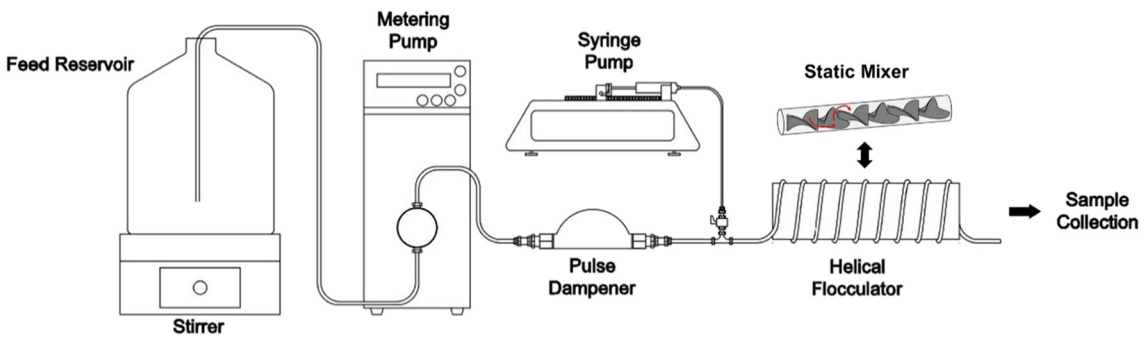

Fig. 2 Schematic of bench-scale system.

line, and the torsion, which describes the out-of-plane twisting of the pipe. To quantify the curvature of each HCTF configuration, eqn (2)–(5) were used, with all parameters defined according to the geometry presented in Fig. 1:[27,47,53]

$$\delta_{nd} = \frac{r_p r_c}{b^2 + {r_c}^2} \quad (2)$$

$$c = \frac{r_p}{r_c} \quad (3)$$

$$R_c = r_c\left[1 + \left(\frac{p}{2\pi r_c}\right)^2\right] \quad (4)$$

$$De = \sqrt{\frac{r_p}{R_c}}Re \quad (5)$$

where δ_{nd} is the dimensionless curvature, c is the curvature ratio, R_c is the modified coil radius of curvature (mm), De is the Dean number, which is the ratio of inertial to viscous forces, Re is the Reynolds number, and b is the pitch slope (mm rad^{-1}). The degree of torsion in the various HCTFs was characterized according to eqn (6)–(8) as defined by Liou,[23] Yamamoto *et al.*,[27] and Mansour *et al.*:[19]

$$\beta_0 = \frac{\lambda}{\sqrt{2\delta_{nd}}} \quad (6)$$

$$\lambda = \frac{b}{r_c} \quad (7)$$

$$\gamma = \frac{p}{2\pi r_c} \quad (8)$$

where β_0 is the torsion parameter, λ is the torsion/curvature ratio, and γ is the dimensionless pitch. HCTF geometrical parameters were again defined according to Fig. 1.

2.4. Floc characterization

2.4.1. Floc sample collection, image acquisition, and processing. Samples acquired from the outlet of the continuous-flow system were immediately taken for analysis. A 1000 μL mechanical pipettor was fitted with a wide orifice pipette tip (Finntip, Thermo Scientific, Hampton, NH) for sample transfer. This approach was previously shown to impart minimal shear on flocs during the transfer of sample.[14] The sample was carefully transferred to a 1 mm × 1 mm gridded Sedgewick-Rafter cell (1801-G20, Wildco, France) for imaging analysis using an optical microscope (Zeiss Standard, Zeiss, Germany) affixed with 3.2× and 10× objective pieces. The ocular tube of the microscope was fitted with a 0.5× reduction lens (A3RDF50, OMAX, WA) and a 10 MP camera (A35100U, OMAX, WA) connected to a computer with image acquisition software (ToupTek, China). Sufficient images were obtained from random locations throughout the counting cell to permit the characterization of 100 flocs for each tested condition. The length of 1 pixel was considered the limit of detection for linear measurements and, using a calibration slide (A36CALM1, OMAX, WA) it was determined to be 0.33 μm. It should be noted that, while large sample sizes are desired to ensure representative characterization of the floc population for each experimental condition, the extensive amount of time required for image acquisition/processing using the microscopic approach imposed practical limitations on the number analyzed. The floc image analysis of a single experiment took half a day's work, longer than conducting the actual flocculation test. Image processing was performed using ImageJ by the U.S. National Institutes of Health (NIH) as in the work by Malkoske.[54] Collected images were processed by subtraction of the image background using a rolling-ball technique with a ball radius of 50–80 pixels and thresholding. The validity of using thresholding in ImageJ for image processing has been previously shown by Balay-Karperien.[55]

2.4.2. Floc size, concentration, and fractal dimension. The ECD of the floc was determined by back calculating for the diameter of a circle with an equivalent area to the floc, as determined from ImageJ analysis of the 2D projection, according to the following equation:[56]

$$ECD = \sqrt{\frac{4A}{\pi}} \quad (9)$$

where ECD is the equivalent circular diameter (μm) and A is the projected area of the floc (μm^2). This procedure is shown graphically in Fig. 3.

Using images of the Sedgewick-Rafter cell acquired with the 3.2× objective, the floc concentration was determined by dividing the number of flocs in each 1 mm × 1 mm grid by the grid volume according to:

$$C_{floc} = \frac{N_{floc}}{V_{grid}} = \frac{N_{floc}}{1\ mm^3} \times \frac{10^3\ mm^3}{1\ cm^3} \times \frac{1\ cm^3}{mL} = 1000 \times N_{floc} \quad (10)$$

where C_{floc} is the estimate for floc concentration (#/mL) and N_{floc} is the number of flocs counted per grid area of the Sedgewick-Rafter cell. The structure of the individual flocs was assessed using the perimeter-based fractal dimension according to the power law relationship presented by Liu *et al.*:[57]

$$A \propto P^{\frac{2}{D_p}} \quad (11)$$

where A is the projected area of the floc (μm^2), P is the floc

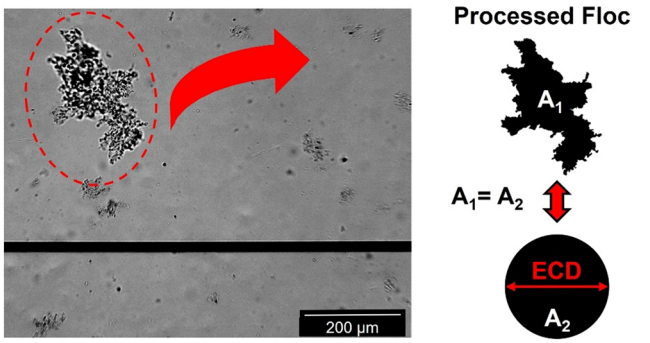

Fig. 3 Microscopic analysis of floc ECD.

perimeter (μm), and D_p is the perimeter-based fractal dimension, which was determined by regression of the log–log plot of floc perimeter *vs.* projected area as in Spicer *et al.*[58] For Euclidian objects such as a perfect sphere, D_p is equal to 1, while for more highly irregular objects approaches a value of 2.

2.5. Statistical analysis for FFD

Statistical treatment of the FFD was performed using JMP® Pro 18 (SAS Institute Inc., Cary, NC). All statistical tests were conducted at a significance level of α = 0.05 and the statistical significance of the regressed models was determined using the analysis of variance (ANOVA) and *F*-test.

3. Results and discussion

3.1. Model fitting and adequacy assessment

A total of 22 experiments were conducted following a replicated three-factor two-level FFD with three center point runs. The experiments were carried out in a randomized order (Table S9) to determine the effects of the factors and their interactions on three responses describing floc characteristics: ECD, D_p, and concentration. The statistical significance of the developed models and individual factors for each of the three response variables considered in the FFD was assessed using the ANOVA and the *F*-test. As shown in Table 3, the *p*-values derived from the *F*-test indicate that the three models are significant with greater than 95% confidence ($p < 0.0035$ in all cases). Among the three response variables, the floc concentration model was found to have the best fit with a coefficient of determination, R^2, greater than 0.88, suggesting that more than 88% of the variability in the response data could be accounted for by the developed model. The regressed model for the floc ECD demonstrated a good fit (R^2 = 0.775), whereas only a moderate fit was found for D_p (R^2 = 0.686). Model adequacy was further evaluated by examining the normality of the residuals. The residual normal quantile plots (see Fig. S3) demonstrated an approximately linear trend for all responses, with residuals falling within the Lilliefors confidence bounds, indicating no significant deviation from normality.[59] Finally, although interaction effects allow for the

Table 3 ANOVA analysis and model adequacy for 2^3 FFD

Response	Factor	Model coefficient estimate	SSE	DF	MSE	*F*-Ratio	*p*-Value
ECD	Intercept	54.6772[c]	—	—	—	—	—
	x_1: Coil pitch	−0.4889	3.824	1	3.824	0.087	0.772
	x_2: Pipe length	9.333	1393.734	1	1393.734	31.744	<0.0001[a]
	x_3: Coil diameter	2.415	93.335	1	93.335	2.126	0.166
	x_1x_2	−6.825	745.265	1	745.265	16.974	0.0009[a]
	x_1x_3	0.906	13.126	1	13.126	0.299	0.593
	x_2x_3	1.248	24.922	1	24.922	0.568	0.463
	Model		2274.206	6	379.034	8.633	0.0004
	Residual error		658.585	15	43.906		
	R^2		0.775				
	RMSE		6.626				
D_p	Intercept	1.5651	—	—	—	—	—
	x_1: Coil pitch	−0.0104	0.001744	1	0.001744	3.766	0.0713[b]
	x_2: Pipe length	−0.0252	0.010188	1	0.010188	21.999	0.0003[a]
	x_3: Coil diameter	−0.00549	0.000482	1	0.000482	1.041	0.3237
	x_1x_2	0.01167	0.002179	1	0.002179	4.705	0.0465[a]
	x_1x_3	0.005095	0.000415	1	0.000415	0.897	0.3586
	x_2x_3	−0.00353	0.000199	1	0.000199	0.430	0.522
	Model		0.01520784	6	0.002535	5.4729	0.0035
	Residual error		0.00694683	15	0.000463		
	R^2		0.686439				
	RMSE		0.02152				
Floc concentration	**Intercept**	15 705.75	—	—	—	—	—
	x_1: Coil pitch	−404.488	2 617 762	1	2 617 762	1.942	0.1838
	x_2: Pipe length	−2229.76	79 549 572	1	79 549 572	59.012	<0.0001[a]
	x_3: Coil diameter	−1725.46	47 635 560	1	47 635 560	35.337	<0.0001[a]
	x_1x_2	−164.26	431 708	1	431 708	0.320	0.5798
	x_1x_3	−756.75	9 162 710	1	9 162 710	6.797	0.0198[a]
	x_2x_3	1071.44	18 367 721	1	18 367 721	13.626	0.0022[a]
	Model		157 765 033	6	26 294 172	19.5056	<0.0001
	Residual error		20 220 466	15	1 348 031		
	R^2		0.88639				
	RMSE		1161.047				

Note: [a] Denotes significant with >95% confidence. [b] Denotes significant with >90% confidence. [c] Model coefficient estimates in terms of coded design variables; SSE = sum of squared errors; DF = degrees of freedom; MSE = mean square error; *F*-ratio is the test statistic for the *F*-test.

developed models to account for some degree of non-linearity, the validity of the linearity assumption inherent to the least-squares regression was also assessed to determine whether pure second-order (quadratic) effects warranted inclusion through an expanded design (*i.e.*, central composite design). Using the procedure outlined by Montgomery,[46] a *t*-test was conducted to test the null hypothesis that the mean of the responses at the center point was equal to that of the factorial points. For all three response variables, the null hypothesis failed to be rejected (SI, section S4.3), indicating that the first-order model with interaction shown in eqn (1) was sufficient to describe the observed relationships.

3.1.1. Main and interaction effects. The least-squares estimates of the coded factor coefficients for the models describing the three response variables are summarized in Table 3. Fig. 4–6 depict the main and interaction effects of factors on the ECD, D_p, and floc concentration, respectively, in the form of three-dimensional surface plots. For the floc ECD, the pipe length and the interaction between pipe length and coil pitch were found to be statistically significant. Considering the interaction factor seen in Fig. 4b as well as the interaction diagrams presented in Fig. S4, the effect of increasing the pipe length is greater at the low factor setting of coil pitch compared to at the high factor setting. Moreover, the effect of coil pitch on the ECD is seen to change depending on the factor setting of pipe length. At the high factor setting for pipe length, the floc ECD increases with decreasing coil pitch, while at the low factor setting the opposite is true. From Fig. 4c, floc ECD is seen to increase primarily as a function of pipe length with minimal interaction between the pipe length and coil diameter as confirmed by a *p*-value of 0.463 (Table 3).

The response surfaces for D_p are presented in Fig. 5 where, it should be noted, the range of the D_p axis was kept at a minimum to better illustrate the effects of flocculator geometry. Floc D_p was found to vary only slightly between

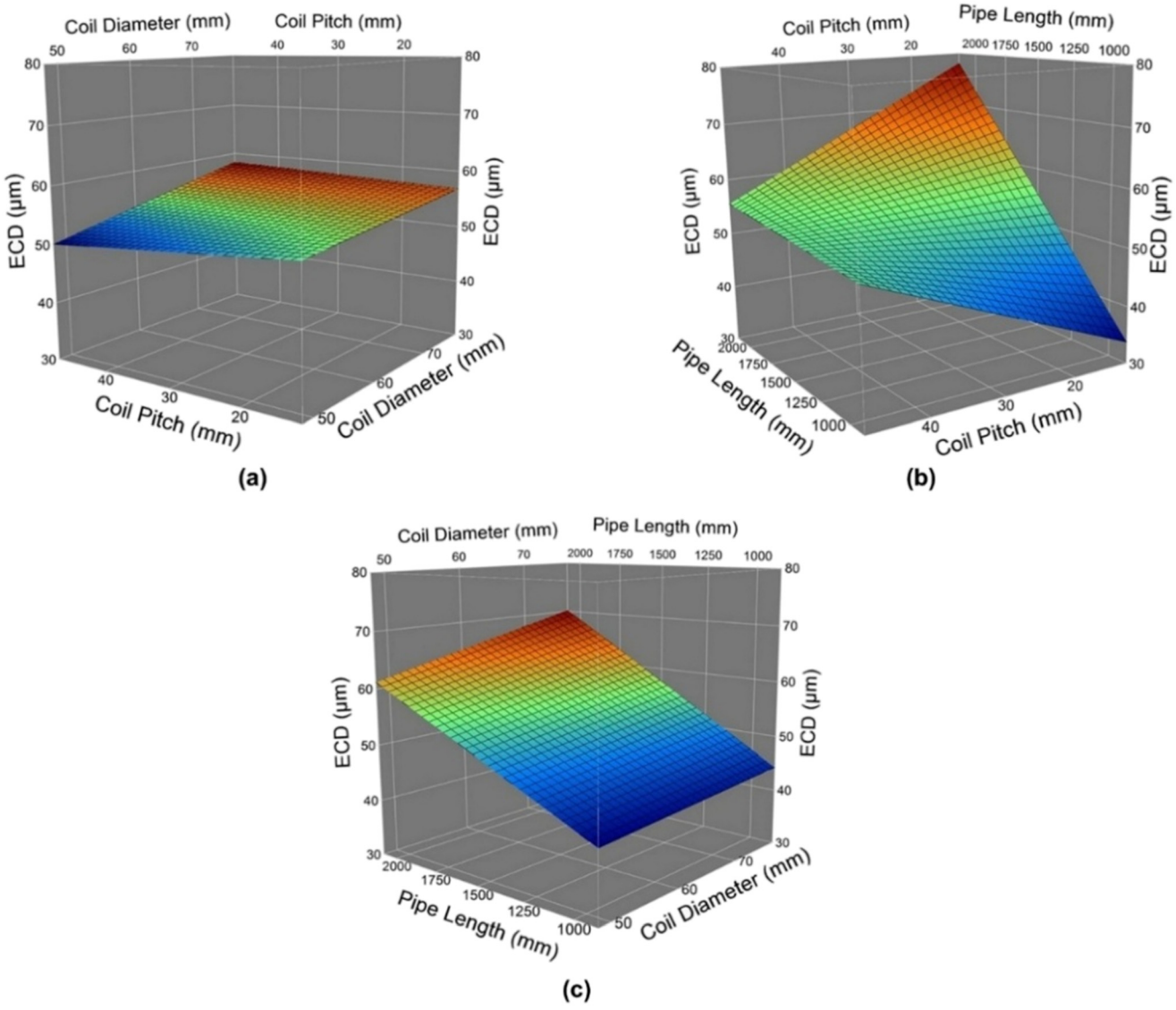

Fig. 4 Response surface plots for ECD showing the interaction between: (a) d_c and p; (b) length and p; (c) length and d_c.

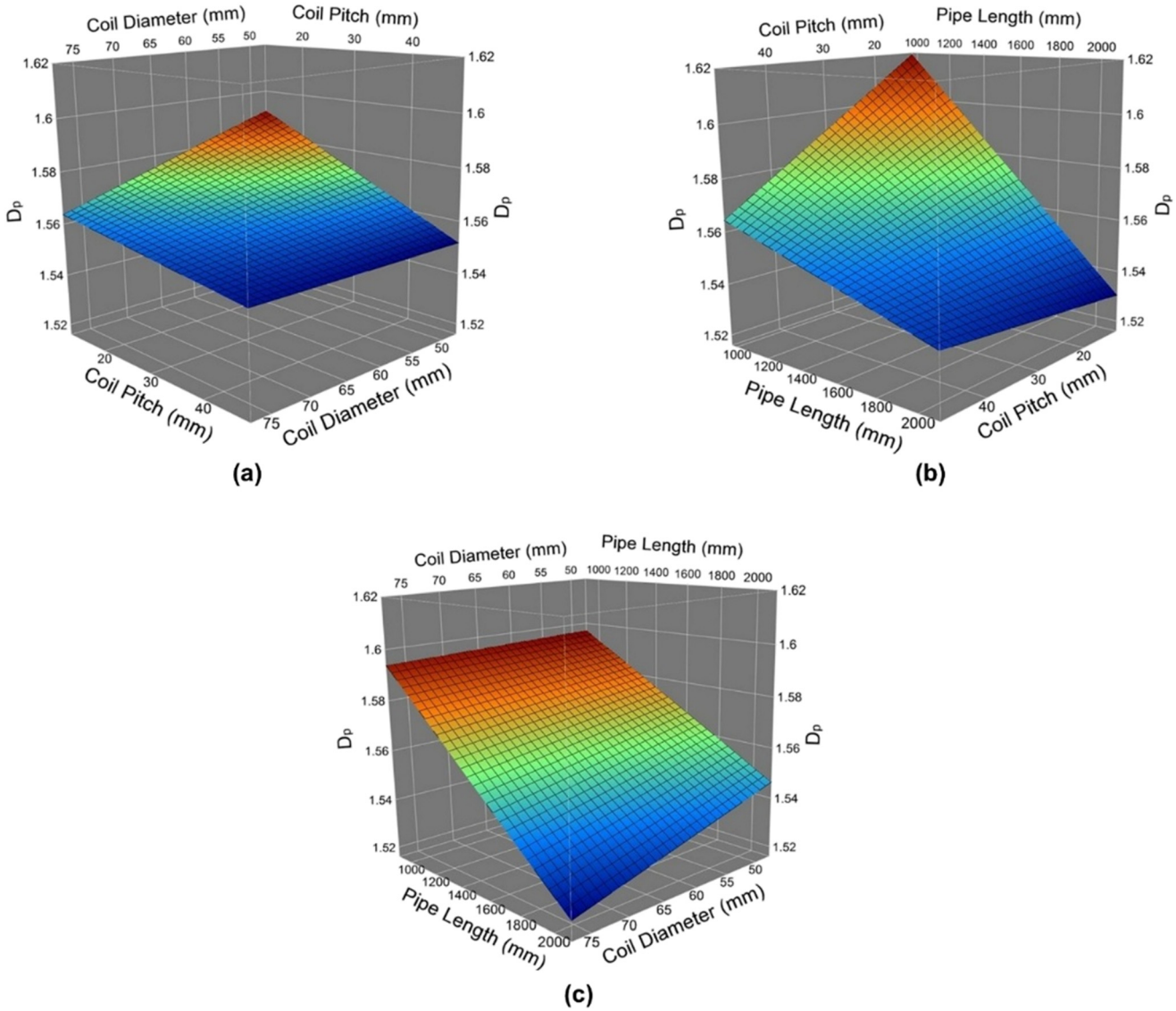

Fig. 5 Response surface plots for D_p showing the interaction between: (a) d_c and p; (b) length and p; (c) length and d_c.

1.512–1.622 (or less than 8%), suggesting that the floc structure remained relatively constant despite changing HCTF geometry (Fig. 5). The use of other fractal definitions, including the one-dimensional and two-dimensional forms (see Jiang[60]), also yielded similar results in that their values were not particularly sensitive to changing HCTF geometry. From Table 3, the main effect of pipe length, as well as its interaction with the coil pitch, were found to have small (but statistically significant) effects, with D_p increasing for smaller pitch and shorter pipe length (Fig. 5b). Recall, a D_p of 1 indicates a perfect Euclidean geometry while more highly irregular objects have a D_p value closer to 2. Thus, it seems that stronger secondary flow produced by more tightly wound HCTFs generated increased particle collision frequency for the aggregation of primary particles, leading to more highly branched floc structures with higher D_p. The effect of pipe length may be related to the HRT: as the residence time inside the flocculator is increased from 1.6 min to 3.2 min (as pipe length increases from 1000 to 2000 mm), the floc structure may re-organize to become more compact with a concomitant decrease in the porosity. In the current study the G value for HCTFs was ~18 s^{-1}, Selomulya *et al.*[61] also reported floc re-organization, without breakup, as flocculation time increased under conditions of moderate mixing intensity (G = 30–80 s^{-1}).

Finally, in the model for floc concentration, the main effects the coil diameter and pipe length were found to be highly significant ($p < 0.001$, Table 3), while the interactions between coil diameter and pipe length ($p = 0.0022$, Table 3) as well as coil diameter and coil pitch ($p = 0.0198$, Table 3) were also found to be significant with greater than 95% confidence. In general (Fig. 6), the floc concentration increased with decreasing pitch, coil diameter, and pipe length. Considering Fig. 6a as well as the interaction diagrams (Fig. S5 and S6), the effect of coil pitch changed depending on the factor setting of the coil diameter. For the

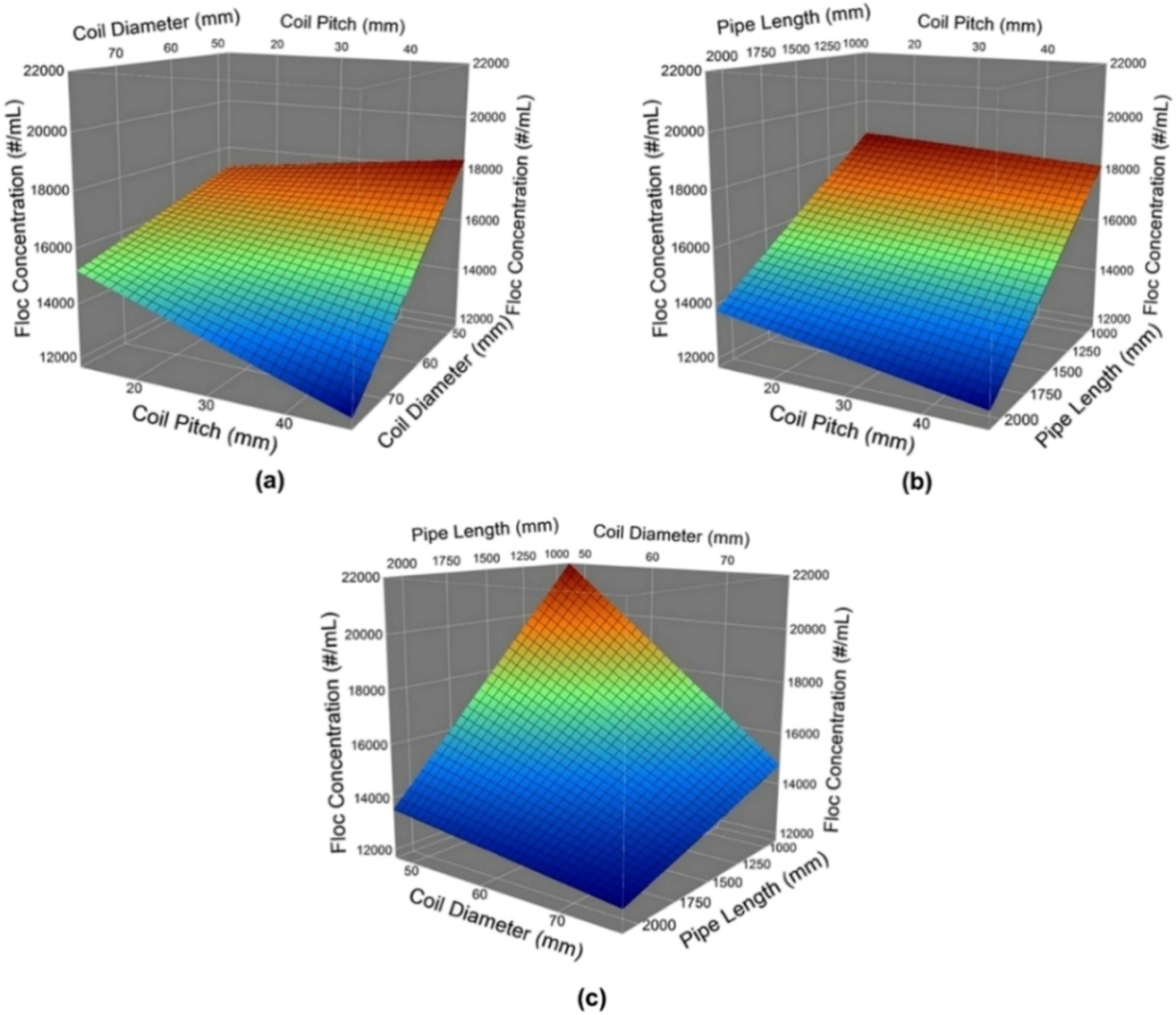

Fig. 6 Response surface plots for floc concentration showing the interaction between: (a) d_c and p; (b) length and p; (c) length and d_c.

low coil diameter conditions, increasing pitch led to a slight increase in floc concentration, whereas at the high setting increasing coil pitch reduced the floc concentration. From Fig. 6c the interaction effect between the coil diameter and pipe length is clearly seen, with simultaneous decreases in both parameters resulting in increasing floc concentration. Comparing these results with those of the model for ECD, it is apparent that the higher pipe length setting yields a longer HRT and permits greater opportunities for floc-floc and floc-particle collisions, forming larger sized flocs (ECD significantly increases with pipe length) in lower concentration.

3.2. Impact of torsion and curvature on HCTF performance

The findings of the FFD were also supported by those of a multivariate regression analysis relating the response variables to measures of torsion and curvature. Recall that these parameters, which were introduced in section 2.3, have been widely used to describe the impact of geometry on flow in helical pipes. Given the strong effect of pipe length on HCTF performance observed in Table 3, the regression analysis was restricted to HCTFs with identical lengths (and thus identical HRTs). For the floc ECD, the effect of coil pitch was seen to change depending on the factor setting of pipe length. This finding was corroborated by the multivariate regression analysis (Fig. 7, Tables S11 and S12) where, at the high factor setting of pipe length, the ECD was found to have strong and statistically significant negative correlations with β_0 (p = 0.06) and γ (p = 0.03), while at the low factor setting (*i.e.*, 1000 mm) had a strong positive correlation with β_0 (p = 0.09) and γ (p = 0.15). The decrease in floc size with increasing torsion, seen for the 2000 mm pipe length setting in the current study (HRT = 3.16 min), was also observed by

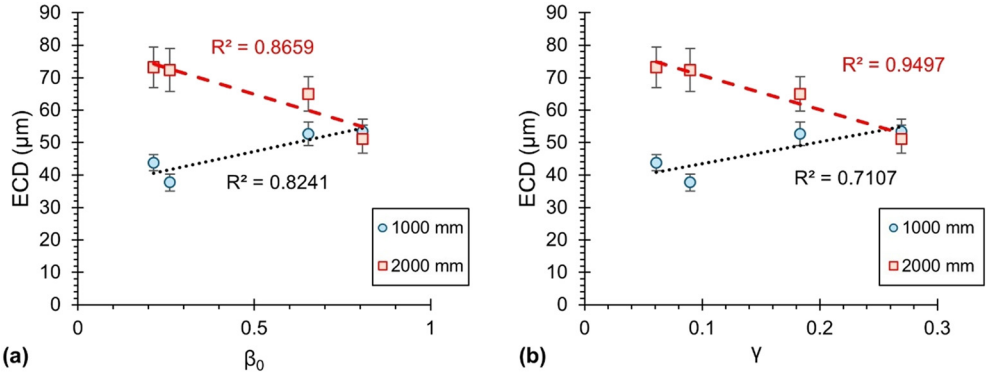

Fig. 7 Relationship between floc ECD and measures of torsion for HCTFs with high and low pipe length settings: (a) ECD *vs.* torsion parameter (β_0); (b) ECD *vs.* dimensionless pitch (γ).

Carissimi *et al.*[33] for an HCTF with a length of 12 m (HRT = 18 s) and operated within the laminar-transitional flow zone. In that study, as γ increased from 0.057–0.452, the observed floc diameter was found to decrease from approximately 3 mm to non-detect. The disparate effect of coil torsion on the ECD for different pipe lengths may be related to the HRT and the number of coil rotations. Tang *et al.*[25] reported that the secondary flow in helically coiled tubes is fully developed within the first rotation while Mansour *et al.*[19] reported that, for conditions similar to those used in the current study (Re $<$ 50 and coil pitch $<$ 60 mm), complete mixing was achieved within approximately three complete revolutions of the HCTF. Thus, for the 2000 mm pipe length, the primary particles experience 7–11 complete rotations of fully developed secondary flow, affording them sufficient opportunity for collisions and aggregate growth. Increasing the coil torsion at this condition serves to destabilize the secondary flow, deteriorating the twin-vortex structure and even delaying their development to higher Re.[27] In contrast, for the 1000 mm condition, the floc growth is limited by the relatively shorter HRT (only 1.6 min) and lower number of rotations (3–5) with fully developed secondary flow. For these HCTFs, it may be that the increased torsion arising from greater coil pitch values led to enhanced vorticity (curl of the local velocity profile) in the pipe, facilitating improved floc growth compared to conditions with lower torsion. The increase in vorticity with torsion was also reported by Wang[62] for low flow conditions (Re $<$ 40) like those used in this bench-scale system.

For floc concentration, the FFD results were also corroborated by the analysis of HCTF curvature (Fig. 8). As the HCTF coil diameter, coil pitch, or the combination of coil pitch and diameter were decreased, the curvature increases and higher floc concentrations were observed. Increased curvature has been shown to generate a larger magnitude centrifugal force, thus a more intense and improved secondary flow that yields more efficient mixing.[18,63] Therefore, for flocculation with the short setting of pipe length where, as noted above, the floc growth can be hindered by the low HRT and number of coil rotations with fully developed flow, it is possible that the improved secondary flow yields greater aggregation efficiency of primary particles, leading to a larger number of detectable/measurable flocs.

3.3. Comparison with alternative C-IN mixer types

Fig. 9 compares the floc ECD, concentration, and D_p of the nine HCTF configurations with those of the batch reactor

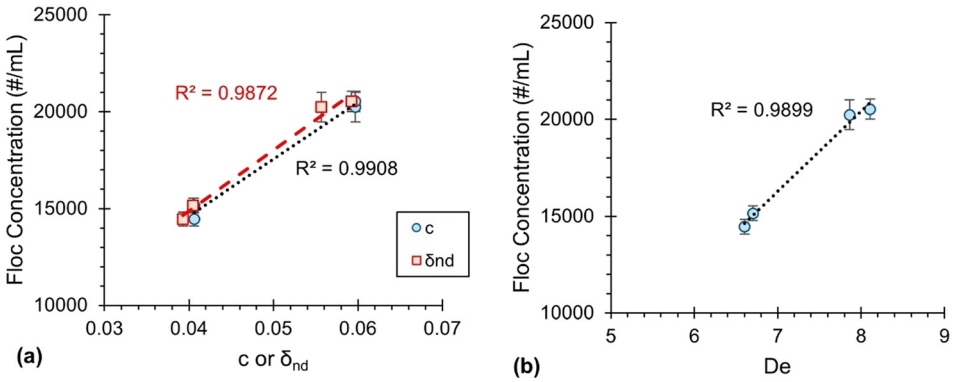

Fig. 8 Relationship between floc concentration and measures of curvature for HCTFs with 1000 mm pipe length: (a) concentration *vs.* curvature ratio (*c*) or dimensionless curvature (δ_{nd}); (b) concentration *vs.* Dean number (De).

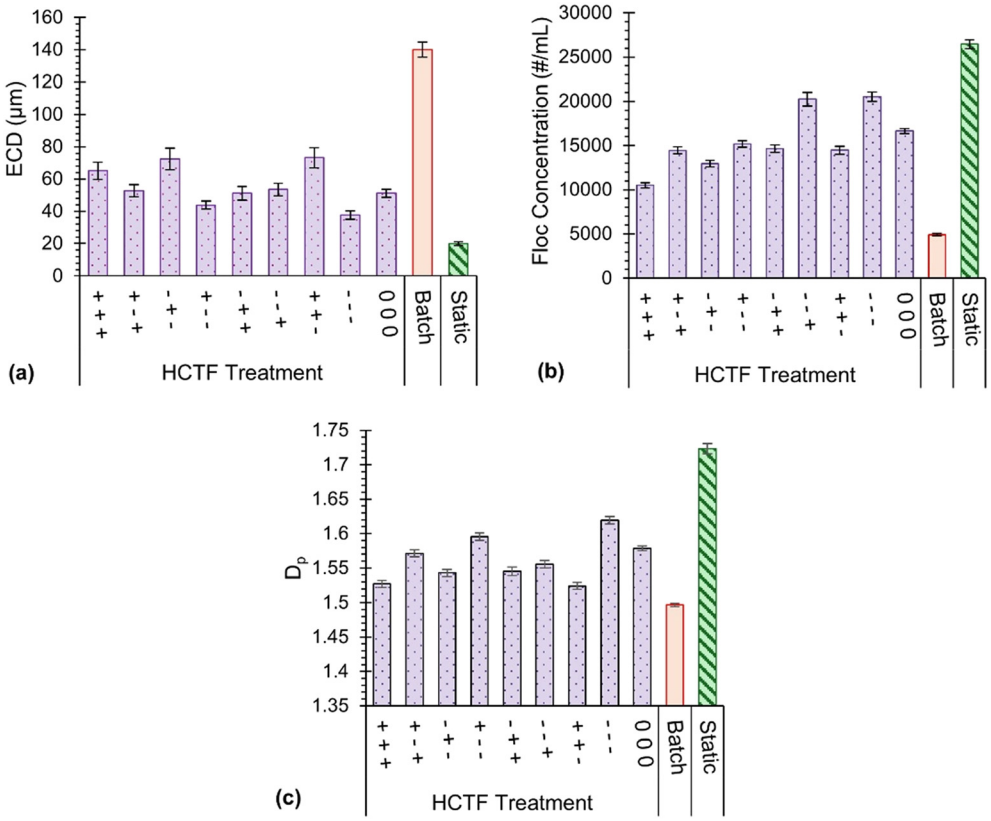

Fig. 9 Comparison of HCTF floc properties with mixing by batch reactor or ISM: (a) ECD; (b) floc concentration; (c) D_p. Note that the HCTF treatments are coded by the factor levels for coil diameter, pipe length, and coil pitch (in that order) where +, 0, and − refer to the high, center-point, and low factor settings, respectively (see Table S9).

and commercial ISM. Although there were significant differences in floc size for the alternative helical flocculators (mean size ranging between 37.7 μm and 73.1 μm), the flocs produced by batch mixing and the ISM were significantly larger (140.1 μm) and smaller (19.8 μm), respectively, than those formed by the HCTFs. Moreover, the size of flocs formed by the batch reactor were found to be stable over a three-hour period following the initial rapid mixing (Fig. S7). When floc concentration was considered, the values for the different HCTFs (10 485–20 529 mL^{-1}) again lay between those for batch (4904 mL^{-1}) and the ISM (26 444 mL^{-1}), although this time the batch mixer yielded the lowest concentration while the ISM yielded the greatest. While statistically significant differences in D_p were observed between the different HCTF configurations and the batch reactor, D_p remained relatively constant and the variations were small, suggesting a similar structure. D_p for the ISM, however, was found to be 6.5–15.2% greater than for the various HCTFs and batch reactor (1.72 *vs.* 1.52–1.59), suggesting a structure with a less compact geometry with a looser and more elongated structure. These findings confirm that, while many C-IN–LPM studies in the literature have used different mixing approaches based on what is available to them or experimentally convenient, the properties of the flocs formed by these mixers differ significantly. As many previous studies have reported that floc size and concentration can impact the properties of the cake layer in C-IN–LPM systems,[34] the degree of fouling reported by bench-scale filtration studies is likely to be impacted by the choice of coagulant mixing. Accordingly, future research should compare the fouling tendency of LPMs pre-treated by C-IN with each of these three mixing approaches. This work should characterize the developed foulant cake so that the measured properties of the flocs and the cake layer can be related to the observed fouling potential.

Comparing the HCTFs with the ISM, both exhibit toroidal flow patterns. In fact, much like HCTFs, Jones *et al.*[64] reported that the helical elements within the ISM produce complex secondary flow patterns with several pairs of counter-rotating vortices formed at the intersection of the elements within the mixer. Despite the apparent similarity in flow pattern, the ISM was seen to have poorer flocculation performance resulting in smaller sized steady-state floc aggregates. As HCTFs with shorter pipe length produced larger flocs (in lower concentration) compared to the ISM, despite having a slightly shorter effective HRT (1.6 min *vs.* 2.58 min), residence time alone could not account for the differences in performance. Rather, the disparity likely reflects differences in the hydrodynamics and secondary flow intensity. It must be acknowledged that, in practice, ISMs are primarily used for coagulant blending with high intensity mixing[65] while HCTFs are employed to promote floc growth

under comparatively low shear. Although the ISM may be a suitable flocculator for bench-scale studies (the manufacturer reports that complete mixing can be achieved by the ISM in the fully laminar flow regime), the slightly larger cross-sectional diameter led to a lower axial flow velocity which likely weakened the secondary flow pattern compared to the HCTFs. Consequently, the potential for cluster–cluster collisions within the ISM would be limited, resulting in the observed smaller sized steady-state floc aggregates. Therefore, ISMs may be more appropriate for bench-scale flocculation studies conducted at higher flowrates, although further investigation is required to confirm this hypothesis and to identify the operational range of flow conditions for which they are appropriate.

The differences in floc properties between the batch reactor and the two continuous-flow mixers is likely due to the absence of rapid (intense) mixing in the latter two alternatives. Based on the aluminum speciation diagram proposed by Amirtharajah and Mills,[66] the coagulation chemistry used in the current study falls within the sweep coagulation zone, however, is influenced by adsorption–destabilization. Although the performance of sweep flocculation is largely independent of the mixing intensity,[67] adsorption destabilization reactions are estimated to occur in less than 1 s. Accordingly, the dispersal of the small coagulant flow across the entire cross-section of the process flow as rapidly as possible is necessary to prevent either incomplete or extensive local adsorption of the metal hydroxide species.[50] For the HCTFs and ISM in the continuous-flow system, the low flowrate condition was possibly inadequate to fully distribute the coagulant within the feedwater. This may have led to local regions where the coagulant concentration was high enough to cause restabilization or too low to destabilize the suspension, resulting in the observed smaller sized floc aggregates as compared to the batch reactor.[68]

The larger flocs formed by the batch-reactor seem to suggest that the inclusion of a dedicated rapid mixing unit is necessary for optimal flocculation performance in continuous-flow bench-scale systems. Accordingly, future work should undertake to develop an inline rapid mixing unit for bench-scale studies and evaluate its impact on the properties of flocs formed by the continuous-flow mixing approaches (*i.e.*, HCTFs and ISM). In addition, although the ISM generated small-sized flocs on its own, its reported ability to achieve complete mixing under firmly laminar conditions suggests that it could be an effective tool for coagulant distribution across the feed upstream of flocculation by HCTFs. This hypothesis should be evaluated by future studies.

3.4. Effect of Reynolds number on HCTF performance

All the experiments presented to this point used the same flowrate and a constant helical tube diameter, thus, they had the same axial flow velocity and Re. To evaluate the impact of Re on the properties of the flocs formed by HCTFs, the system was operated at three different flowrates. Fig. 10 compares the ECD and floc concentration found for the HCTF at the center point of the FFD (HRT = 2.4 min, Re = 33.3) with those for the same HCTF operated at flowrates of 10 mL min^{-1} (HRT = 1.2 min, Re = 66.6) and 20 mL min^{-1} (HRT = 0.6 min, Re = 133.3). While the D_p was found to vary narrowly between 1.55–1.6 for the three studied Re values, the mean ECD was found to initially increase (from 51.1 μm to 108.8 μm) as the Re increased from 33.3 to 66.6, before decreasing to 33.9 μm as the Re was further increased to 133.3. Opposite to ECD, the floc concentration initially decreased with increasing Re before increasing as the Re was increased from 66.6 to 133.3. This unimodal pattern was also observed in the studies by De Oliveira and Teixeira[29] and De Oliveira *et al.*[69] where the turbidity removal efficiency (TRE) was measured as a surrogate for HCTF flocculation performance at different flowrates and HRTs. In the current study, given that the floc fractal dimension remains nearly constant for the three different Re conditions, achieved by changing the flowrate, the ECD would be expected to represent the TRE given the well-established relationships between TRE and settling velocity as well as settling velocity and size/fractal dimension.[31,32] Given that the variation in floc ECD was much greater for changing Re compared to the average effect of pipe length (*i.e.*, $\overline{ECD_{2000}} - \overline{ECD_{1000}} = 18.5$ μm), which was shown to be the most significant HCTF geometrical parameter, the tubular flow Re (which is directly related to the flowrates studied) should be considered as the most important variable in the design of HCTFs.

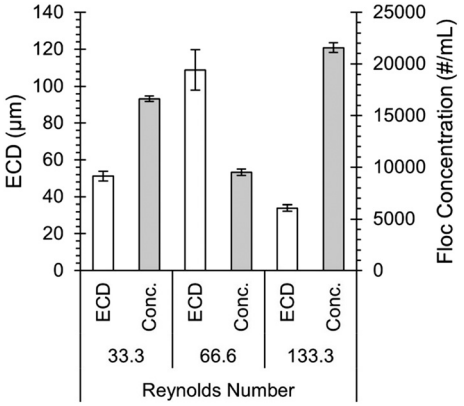

Fig. 10 Effect of Reynolds number on ECD and floc concentration at FFD center point (length = 1500 mm; d_c = 67.5 mm; p = 30 mm).

The unimodal pattern is likely the result of a trade-off between the mixing intensity and the HRT of the flocculator. As the Re is increased from 33.3 to 66.6, increasing Dean number (7.25 → 14.49) and G value (18 s^{-1} → 36 s^{-1}) suggests a stronger secondary flow, which should lead to improved mixing characteristics. In fact, Serra *et al.*[70] reported that floc size increased with G values up to ~30 s^{-1} due to aggregation dominated flocculation. This was seen in the current study by the increased floc ECD and the concomitant lower floc

concentration as more primary particles and small flocs are aggregated into larger sized flocs. As the Re increased to 133.3 the secondary flow pattern is again strengthened (De = 14.49 → 29), however, the magnitude of the Dean number actually exceeds the region ($5 \leq De \leq 21$) identified by Mansour *et al.*[71] for optimal mixing across a wide range of HCTF geometries. Moreover, the G value, which reached ~75 s^{-1}, suggests shear-induced breakage of floc aggregates, which led to smaller sized particles as in the study by Yu *et al.*[72] The increased flowrate associated with the highest Re also led to a decrease in flocculator HRT to only 0.6 min, which affords little opportunity for collisions between the flocs, yielding a suspension with a larger concentration of small sized flocs. This hypothesis should be confirmed by future testing which compares the effect of varying flowrate for HCTFs of the same geometry, but also with the same HRT.

3.5. Experimental design guidelines

As shown in this study, irrespective of the geometry, HCTFs are an effective means to achieve flocculation in bench-scale continuous-flow systems with low Re. A distinct advantage of HCTFs is the flexibility that they provide in design, with a completely customizable geometry capable of producing flocs of differing character according to the downstream technology choice and experimental requirements. The system flowrate (*i.e.*, Re) was shown to exert the greatest effect on floc ECD, with the trade-off between shear intensity and mixing HRT governing the potential for floc agglomeration and growth. Therefore, the design of HCTFs should select pipe diameter accordingly to provide Re, De, G, and HRT values (for the corresponding flowrate) that facilitate the formation of flocs with the desired properties. The helical pipe length and, by extension, HRT were found to be the geometrical parameters that have the most significant impact on floc ECD and thus should also be carefully considered in future work. It is suggested that the scalability of these guidelines also be tested in full-scale units.

For LPM pretreatment, Malkoske *et al.*[14] reported that increased floc concentration improved the hydraulic reversibility of fouling and the release of retained NOM from the membrane surface. However, Amjad *et al.*[34] noted the importance of mass loading during filtration and larger floc sizes are known to reduce the cake resistance to filtration.[73] For conventional coagulation/flocculation/sedimentation large sized flocs are also desired to enable rapid settling times.[4] Therefore, to produce the largest sized flocs HCTFs with longer pipes (higher HRTs) and small coil pitch values should be specified, although, for LPM pretreatment applications the inverse proportionality between the floc ECD and floc concentration should be kept in mind. According to the results of section 3.4, the HCTF pipe diameter should be selected to provide Re, De and G values near 67, 15 and 30 s^{-1}, respectively, which were optimal for floc growth. These conditions produced flocs with an average ECD greater than 100 μm, which Edzwald[74] as well as Edzwald and Haarhoff[75] have noted is the minimum size required to provide reasonable settling velocities in downstream settling basins. For LPM filtration applications, Park *et al.*[76] have also reported that the specific cake layer resistance is minimized for flocs larger than 100 μm in size.

4. Conclusions

In this study, as a result of their strong secondary flow pattern, HCTFs were shown to provide sufficient mixing for good floc development under laminar flow conditions with Reynolds numbers as low as 33.3. Through the use of a 2^3 FFD, this work represents the first effort to comprehensively and systematically investigate the impact of helical geometry on the properties of flocs formed in continuous-flow coagulation systems typical of those used for LPM fouling mitigation studies. The performance of the HCTFs was additionally compared with that of a commercial ISM and batch coagulation reactor, which have also been extensively used in C-IN–LPM studies. The results of the study may be summarized as:

1. Helical geometry was confirmed to have a statistically significant impact on the properties of flocs formed by HCTFs. The floc size was significantly impacted by the pipe length and the interaction between pipe length and coil pitch. When the floc concentration was considered, the main effects of coil diameter and pipe length, their interaction, as well as the interaction between coil diameter and coil pitch were the significant factors. In contrast, the floc structure remained relatively constant for all geometries considered, with only the pipe length and its interaction with coil pitch exhibiting small, but statistically significant, effects.

2. The variation in floc properties produced by HCTFs in the FFD could also be correlated well to measures of pipe curvature and torsion. For HCTFs at the high factor setting of pipe length, the torsion parameter displayed a strong negative correlation with floc size, likely due to its disruptive effect on the secondary flow pattern. In contrast, for HCTFs with a short pipe length, increased torsion led to greater ECD possibly due to increased vorticity in the secondary flow.

3. Statistically significant differences existed in the mean floc ECD and concentration for the three mixer types investigated with batch mixing yielding the largest flocs in the lowest concentration, while the commercial ISM produced the smallest flocs in the largest concentration. The flocs produced by the ISM were also found to have a significantly looser structure compared to those of the HCTFs and batch reactor.

4. Compared to parameters describing helical geometry, Reynolds number exhibited the greatest impact on floc properties. For three different flowrates with Reynolds numbers between 33.3 and 133.3, the ECD initially showed an increasing, then decreasing trend, while the floc concentration changed in inverse. The unimodal pattern was likely the result of a trade-off between the mixing intensity (G

value), the secondary flow strength (De number), and the flocculation HRT. Initial floc size increase was promoted by stronger secondary flow (De 7.25 → 14.49) and aggregation-dominated flocculation ($G < \sim 30\ s^{-1}$) at reasonable HRTs, however, shear induced floc breakup ($G \sim 75\ s^{-1}$) and decreasing flocculation HRT (2.4 min → 0.6 min) likely led to smaller flocs in greater concentrations as the system flowrate increased. Accordingly, the impact of Reynolds number for HCTFs with constant HRT should be studied further. The Reynolds number is critical to the design of future HCTFs and appropriate selection of pipe diameter is required for the system to operate within optimal regions of De, G, and HRT.

Future studies should investigate how the altered floc properties seen for each mixing approach impact LPM fouling in the integrated C-IN–LPM system. Moreover, it would be of interest to characterize the fouling layer in the C-IN–LPM system so that the observed fouling potential and cake layer properties may be related to the characteristics of the flocs formed by each mixing type. Finally, rapid mixing in the batch coagulation approach seemed to have an important effect on floc growth. Accordingly, future work should consider the development of an inline rapid mixing unit with reasonable HRTs for bench-scale systems and evaluate its impact on floc properties and membrane fouling for continuous-flow C-IN with the HCTFs and ISM used in this study.

Author contributions

Joseph D. Ladouceur: conceptualization, methodology, investigation, formal analysis, writing – original draft, visualization Roberto M. Narbaitz: conceptualization, writing – review & editing, funding acquisition, supervision, resources Christopher Q. Lan: conceptualization, writing – review & editing, funding acquisition, supervision.

Conflicts of interest

The authors declare that they have no known competing financial interests or personal relationships that could have influenced the work reported in this paper.

Data availability

Data generated in this study can be found in the published article and its supplementary information (SI) files.

Supplementary information is available. See DOI: https://doi.org/10.1039/d6ew00221h.

Acknowledgements

This work was supported by the Natural Sciences and Engineering Research Council of Canada (NSERC) under grant RGPIN 2018-06571 as well as the NSERC Canada Graduate Scholarship- Doctoral Program (ID 579943-2023). The authors would also like to acknowledge financial support provided to the lead author by the American Membrane Technology Association (AMTA) through their Ian C. Watson Fellowship and by the American Water Works Association (AWWA) through the Dr. James K. Edzwald Scholarship. Finally, the authors extend their thanks to Catherine Brosseau (Kemira Water Solutions Canada) for providing coagulants for this study as well as Mr. Julian Fino for his help in the lab.

References

1 G. K. Pearce, Is the Water Membrane Market in a State of Flux?, *WaterWorld*, 2018, p. 16201283, https://www.waterworld.com/drinking-water-treatment/article/16201283/is-the-water-membrane-market-in-a-state-of-flux.
2 K. Kinser, Membrane Filtration: Past, Present, and Future, *J. AWWA*, 2021, **113**, 72–75.
3 M. T. Alresheedi, S. L. D. Kenari, B. Barbeau and O. D. Basu, Flux modulation: A novel approach for ultrafiltration fouling control, *J. Water Process Eng.*, 2022, **46**, 102551.
4 J. D. Ladouceur, R. M. Narbaitz and C. Q. Lan, Dissolved air flotation pretreatment for low-pressure membranes in water treatment: A review of fouling mitigation and product water quality, *J. Water Process Eng.*, 2023, **56**, 104391.
5 F. Zietzschmann, M. Ernst, M. Godehardt, H. Paar, X. Zheng and M. Jekel, Linking UF reversible and irreversible fouling to the water quality of surface water and treated municipal wastewater, *Desalin. Water Treat.*, 2014, **52**, 7598–7608.
6 G. Amy, Fundamental understanding of organic matter fouling of membranes, *Desalination*, 2008, **231**, 44–51.
7 AWWA, Committee Report: Recent advances and research needs in membrane fouling, *J. AWWA*, 2005, **97**, 79–89.
8 K. J. Howe, A. Marwah, K.-P. Chiu and S. S. Adham, Effect of coagulation on the size of MF and UF membrane foulants, *Environ. Sci. Technol.*, 2006, **40**, 7908–7913.
9 K. Kimura and K. Kume, Irreversible fouling in hollow-fiber PVDF MF/UF membranes filtering surface water: Effects of precoagulation and identification of the foulant, *J. Membr. Sci.*, 2020, **602**, 117975.
10 H. Huang, K. Schwab and J. G. Jacangelo, Pretreatment for low pressure membranes in water treatment: A review, *Environ. Sci. Technol.*, 2009, **43**, 3011–3019.
11 T. A. Malkoske, P. R. Bérubé and R. C. Andrews, Coagulation/flocculation prior to low pressure membranes in drinking water treatment: A review, *Environ. Sci.: Water Res. Technol.*, 2020, **6**, 2993–3023.
12 American Water Works Association, *Manual of Water Supply Practices - M62: Membrane Applications for Water Reuse*, American Water Works Association, Denver, CO, 1st edn, 2018.
13 G. Kamińska, W. Pronk and J. Traber, Effect of coagulant dose and backflush pressure on NOM membrane fouling in inline coagulation-ultrafiltration, *Desalin. Water Treat.*, 2020, **199**, 188–197.
14 T. A. Malkoske, P. R. Bérubé and R. C. Andrews, Impact of extended versus typical rapid mixing HRTs on continuous-flow coagulation-ultrafiltration, *Sep. Purif. Technol.*, 2023, **319**, 124041.

15 J. D. Ladouceur and R. M. Narbaitz, Reduced low–pressure membrane fouling by inline coagulation pretreatment for a colored river water, *Membranes*, 2022, **12**, 1028.
16 J. D. Ladouceur and R. M. Narbaitz, Comparing sedimentation, flotation, and inline pre-treatment for low-pressure membrane fouling reduction, *J. Environ. Eng.*, 2023, **149**(4), 04023002.
17 C. K. Tang, N. M. Peleato, P. R. Bérubé and R. C. Andrews, Impact of low coagulant dosages on protein fouling of ultrafiltration membranes, *J. Water Process Eng.*, 2019, **31**, 100801.
18 M. Mansour, Z. Liu, G. Janiga, K. D. P. Nigam, K. Sundmacher, D. Thévenin and K. Zähringer, Numerical study of liquid-liquid mixing in helical pipes, *Chem. Eng. Sci.*, 2017, **172**, 250–261.
19 M. Mansour, P. Khot, D. Thévenin, K. D. P. Nigam and K. Zähringer, Optimal Reynolds number for liquid-liquid mixing in helical pipes, *Chem. Eng. Sci.*, 2020, **214**, 114522.
20 C. Zhang, A. R. Ferrell and K. Nandakumar, Study of a toroidal-helical pipe as an innovative static mixer in laminar flows, *Chem. Eng. J.*, 2019, **359**, 446–458.
21 T. J. Huttl and R. Friedrich, Infuence of curvature and torsion on turbulent flow in helically coiled pipes, *Int. J. Heat Fluid Flow*, 2000, 345–353.
22 A. Cioncolini and L. Santini, An experimental investigation regarding the laminar to turbulent flow transition in helically coiled pipes, *Exp. Therm. Fluid Sci.*, 2006, **30**, 367–380.
23 T. M. Liou, Flow visualization and LDV measurement of fully developed laminar flow in helically coiled tubes, *Exp. Fluids*, 1992, **13**, 332–338.
24 M. Sartori, D. S. Oliveira, E. C. Teixeira, W. B. Rauen and N. C. Reis, CFD modelling of helically coiled tube flocculators for velocity gradient assessment, *J. Braz. Soc. Mech. Sci. Eng.*, 2015, **37**, 187–198.
25 L. Tang, Y. Tang and S. Parameswaran, A numerical study of flow characteristics in a helical pipe, *Adv. Mech. Eng.*, 2016, **8**, 168781401666024.
26 K. Yamamoto, T. Akita, H. Ikeuchi and Y. Kita, Experimental study of the flow in a helical circular tube, *Fluid Dyn. Res.*, 1995, **16**, 237–249.
27 K. Yamamoto, A. Aribowo, Y. Hayamizu, T. Hirose and K. Kawahara, Visualization of the flow in a helical pipe, *Fluid Dyn. Res.*, 2002, **30**, 251–267.
28 G. H. Cahyana, P. Suwandhi and T. Mulyani, Novel helical or coiled flocculator for turbidity reduction in drinking water treatment: a performance study, *IOP Conf. Ser. Earth Environ. Sci.*, 2021, **623**, 012009.
29 D. S. De Oliveira and E. C. Teixeira, Experimental evaluation of helically coiled tube flocculators for turbidity removal in drinking water treatment units, *Water SA*, 2017, **43**, 378.
30 M. Maraschin, K. F. S. H. Ferrari, A. P. H. da Silva and E. Carissimi, Aluminum sludge thickening: Novel helical pipes for aggregation by dual flocculation and thickening by filtration applied to water treatment plants, *Sep. Purif. Technol.*, 2020, **241**, 116560.
31 A. Vahedi and B. Gorczyca, Application of fractal dimensions to study the structure of flocs formed in lime softening process, *Water Res.*, 2011, **45**, 545–556.
32 A. Vahedi and B. Gorczyca, Predicting the settling velocity of flocs formed in water treatment using multiple fractal dimensions, *Water Res.*, 2012, **46**, 4188–4194.
33 E. Carissimi, D. G. Sanagiotto, E. B. C. Schettini and J. Rubio, Revisiting coiled flocculator performance for particle aggregation, *Water Environ. Res.*, 2018, **90**, 322–328.
34 H. Amjad, Z. Khan and V. V. Tarabara, Fractal structure and permeability of membrane cake layers: Effect of coagulation–flocculation and settling as pretreatment steps, *Sep. Purif. Technol.*, 2015, **143**, 40–51.
35 J. Nan, M. Yao, Q. Li, D. Zhan, T. Chen, Z. Wang and H. Li, The role of shear conditions on floc characteristics and membrane fouling in coagulation/ultrafiltration hybrid process – the effect of flocculation duration and slow shear force, *RSC Adv.*, 2016, **6**, 163–173.
36 P. Du, X. Li, Y. Yang, Z. Su, H. Li, N. Wang, T. Guo, T. Zhang and Z. Zhou, Optimized coagulation pretreatment alleviates ultrafiltration membrane fouling: The role of floc properties and slow-mixing speed on mechanisms of chitosan-assisted coagulation, *J. Environ. Sci.*, 2019, **82**, 82–92.
37 X. Shen, B. Gao, K. Guo and Q. Yue, Characterization and influence of floc under different coagulation systems on ultrafiltration membrane fouling, *Chemosphere*, 2020, **238**, 124659.
38 Y. Liu, Z. Wang, M. Xu, F. Qi, C. Li, D. Sun, J. Nan, W. Li, X. Guan and A. Ikhlaq, Unveiling the role of cake layer in coagulation-ultrafiltration on membrane fouling and emerging application as dynamic membrane before ultrafiltration, *Sep. Purif. Technol.*, 2024, **350**, 127932.
39 F. García-Ávila, D. Tenesaca-Pintado, F. Novoa-Zamora, E. A. Alfaro-Paredes, A. Avilés-Añazco, A. Guanuchi-Quito, M. D. Tonon-Ordoñez and C. Zhindón-Arévalo, Vertical tubular flocculator: Alternative technology for the improvement of drinking water treatment processes in rural areas, *J. Environ. Manage.*, 2023, **331**, 117342.
40 M. Winterdahl, *Doctoral Dissertation*, Swedish University of Agricultural Science, 2013.
41 D. S. Mallya, S. Abdikheibari, L. F. Dumée, S. Muthukumaran, W. Lei and K. Baskaran, Removal of natural organic matter from surface water sources by nanofiltration and surface engineering membranes for fouling mitigation – A review, *Chemosphere*, 2023, **321**, 138070.
42 M. Schulz, A. Soltani, X. Zheng and M. Ernst, Effect of inorganic colloidal water constituents on combined low-pressure membrane fouling with natural organic matter (NOM), *J. Membr. Sci.*, 2016, **507**, 154–164.
43 J. C. Crittenden, R. R. Trussell, D. W. Hand, K. J. Howe and G. Tchobanoglous, *Water treatment: Principles and design*, McGraw-Hill, New York, NY, 3rd edn, 2012.
44 J. K. Edzwald and J. E. Tobiason, Enhanced coagulation: US requirements and a broader view, *Water Sci. Technol.*, 1999, **40**, 63–70.
45 M. T. Alresheedi and O. D. Basu, Effects of feed water temperature on irreversible fouling of ceramic ultrafiltration membranes, *J. Water Process Eng.*, 2019, **31**, 100883.

46 D. C. Montgomery, *Design and Analysis of Experiments*, Wiley, Hoboken, NJ, USA, 10th edn, 2020.
47 M. Mansour, K. Zähringer, K. D. P. Nigam, D. Thévenin and G. Janiga, Multi-objective optimization of liquid-liquid mixing in helical pipes using genetic algorithms coupled with computational fluid dynamics, *Chem. Eng. J.*, 2020, **391**, 123570.
48 I. C. Tse, K. Swetland, M. L. Weber-Shirk and L. W. Lion, Method for quantitative analysis of flocculation performance, *Water Res.*, 2011, **45**, 3075–3084.
49 W. Yu, J. Gregory, L. C. Campos and N. Graham, Dependence of floc properties on coagulant type, dosing mode and nature of particles, *Water Res.*, 2015, **68**, 119–126.
50 J. Bratby, *Coagulation and Flocculation in Water and Wastewater Treatment*, IWA Publishing, London, UK, 3rd edn, 2016.
51 M.-A. A. M. Neama, W. A. Elbarki, M. Fayed and S. Aly, Upgrading the eastern wastewater treatment plant effluent quality in Egypt for reuse by means of in-line coagulation followed by ultrafiltration, *Water Pract. Technol.*, 2024, **19**, 4754–4772.
52 N. M. Peleato, R. L. Legge and R. C. Andrews, Characterization of UF foulants and fouling mechanisms when applying low in-line coagulant pre-treatment, *Water Res.*, 2017, **126**, 1–11.
53 P. Mishra and S. N. Gupta, Momentum Transfer in Curved Pipes. 1. Newtonian Fluids, *Ind. Eng. Chem. Process Des. Dev.*, 1979, **18**, 130–137.
54 T. A. Malkoske, *PhD thesis*, University of Toronto, 2023.
55 A. Balay-Karperinen, *MSc*, Charles Sturt University, 2004.
56 P. Jarvis, B. Jefferson and S. A. Parsons, Measuring Floc Structural Characteristics, *Rev. Environ. Sci. Biotechnol.*, 2005, **4**, 1–18.
57 Y. Liu, X. Zhang, W. Jiang, M. Wu and Z. Li, Comprehensive review of floc growth and structure using electrocoagulation: Characterization, measurement, and influencing factors, *Chem. Eng. J.*, 2021, **417**, 129310.
58 P. T. Spicer, W. Keller and S. E. Pratsinis, The Effect of Impeller Type on Floc Size and Structure during Shear-Induced Flocculation, *J. Colloid Interface Sci.*, 1996, **184**, 112–122.
59 W. J. Conover, *Practical Nonparametric Statistics*, Wiley, Hoboken, NJ, USA, 3rd edn, 1999.
60 Q. Jiang, *PhD thesis*, The University of Arizona, 1993.
61 C. Selomulya, R. Amal, G. Bushell and T. D. Waite, Evidence of Shear Rate Dependence on Restructuring and Breakup of Latex Aggregates, *J. Colloid Interface Sci.*, 2001, **236**, 67–77.
62 C. Y. Wang, On the low-Reynolds-number flow in a helical pipe, *J. Fluid Mech.*, 1981, **108**, 185–194.
63 V. Kumar, M. Aggarwal and K. D. P. Nigam, Mixing in curved tubes, *Chem. Eng. Sci.*, 2006, **61**, 5742–5753.
64 S. C. Jones, F. Sotiropoulos and A. Amirtharajah, Numerical modeling of helical static mixers for water treatment, *J. Environ. Eng.*, 2002, **128**, 431–440.
65 J. K. Edzwald, Coagulant mixing revisited: theory and practice, *J. Water Supply: Res. Technol.–AQUA*, 2013, **62**, 67–77.
66 A. Amirtharajah and K. M. Mills, Rapid-mix design for mechanisms of alum coagulation, *J. AWWA*, 1982, **74**, 210–216.
67 S. Kawamura, *Integrated Design and Operation of Water Treatment Facilities*, John Wiley & Sons, New York, NY, 2000.
68 R. D. Letterman, J. E. Quon and R. S. Gemmell, Influence of rapid-mix parameters on flocculation, *J. AWWA*, 1973, **65**, 716–722.
69 D. S. De Oliveira, E. C. Teixeira and C. B. Donadel, Novel approaches for predicting efficiency in helically coiled tube flocculators using regression models and artificial neural networks, *Water Environ. J.*, 2020, **34**, 550–562.
70 T. Serra, J. Colomer and B. E. Logan, Efficiency of different shear devices on flocculation, *Water Res.*, 2008, **42**, 1113–1121.
71 M. Mansour, D. Thévenin, K. D. P. Nigam and K. Zähringer, Generally-valid optimal Reynolds and Dean numbers for efficient liquid-liquid mixing in helical pipes, *Chem. Eng. Sci.*, 2019, **201**, 382–385.
72 W. Yu, J. Gregory, L. Campos and G. Li, The role of mixing conditions on floc growth, breakage and re-growth, *Chem. Eng. J.*, 2011, **171**, 425–430.
73 J. Guan, R. Amal and T. D. Waite, Effect of aggregate size and structure on specific resistance of biosolids filter cakes, *Water Sci. Technol.*, 2001, **44**, 215–220.
74 *Water quality & treatment: A handbook on drinking water*, ed. J. K. Edzwald, American Water Works Association, Denver, CO, 6th edn, 2011.
75 J. K. Edzwald and J. Haarhoff, *Dissolved Air Flotation for Water Clarification*, McGraw-Hill, New York, NY, 1st edn, 2012.
76 P.-K. Park, C.-H. Lee and S. Lee, Permeability of Collapsed Cakes Formed by Deposition of Fractal Aggregates upon Membrane Filtration, *Environ. Sci. Technol.*, 2006, **40**, 2699–2705.

